

An Fc-free EGFR-specific 4-1BB-agonistic Trimerbody Displays Broad Antitumor Activity in Humanized Murine Cancer Models without Toxicity

Marta Compte¹, Seandean L. Harwood², Ainhoa Erce-Llamazares^{1,3,4}, Antonio Tapia-Galisteo⁵, Eduardo Romero⁶, Irene Ferrer^{7,8}, Eva M. Garrido-Martin^{7,8}, Ana B. Enguita^{9,10}, Maria C. Ochoa¹¹, Belén Blanco^{3,4}, Marta Oteo⁶, Nekane Merino¹², Daniel Nehme-Álvarez^{3,4}, Oana Hangiu^{3,4}, Carmen Domínguez-Alonso^{3,4}, Manuela Zonca¹, Angel Ramírez-Fernández^{3,4}, Francisco J. Blanco¹³, Miguel A. Morcillo⁶, Ines G. Muñoz¹⁴, Ignacio Melero^{8,11,15,16}, José L. Rodríguez-Peralta^{8,9,10,17}, Luis Paz-Ares^{7,8,18,19}, Laura Sanz⁵, and Luis Alvarez-Vallina^{2,3,4}

ABSTRACT

Purpose: The induction of 4-1BB signaling by agonistic antibodies can drive the activation and proliferation of effector T cells and thereby enhance a T-cell-mediated antitumor response. Systemic administration of anti-4-1BB-agonistic IgGs, although effective preclinically, has not advanced in clinical development due to their severe hepatotoxicity.

Experimental Design: Here, we generated a humanized EGFR-specific 4-1BB-agonistic trimerbody, which replaces the IgG Fc region with a human collagen homotrimerization domain. It was characterized by structural analysis and *in vitro* functional studies. We also assessed pharmacokinetics, antitumor efficacy, and toxicity *in vivo*.

Results: In the presence of a T-cell receptor signal, the trimerbody provided potent T-cell costimulation that was strictly dependent

on 4-1BB hyperclustering at the point of contact with a tumor antigen-displaying cell surface. It exhibits significant antitumor activity *in vivo*, without hepatotoxicity, in a wide range of human tumors including colorectal and breast cancer cell-derived xenografts, and non-small cell lung cancer patient-derived xenografts associated with increased tumor-infiltrating CD8⁺ T cells. The combination of the trimerbody with a PD-L1 blocker led to increased IFN γ secretion *in vitro* and resulted in tumor regression in humanized mice bearing aggressive triple-negative breast cancer.

Conclusions: These results demonstrate the nontoxic broad antitumor activity of humanized Fc-free tumor-specific 4-1BB-agonistic trimerbodies and their synergy with checkpoint blockers, which may provide a way to elicit responses in most patients with cancer while avoiding Fc-mediated adverse reactions.

Introduction

Modulating immune responses using mAbs is one of the most promising approaches for cancer immunotherapy (1). Probably most well known is the mAb-mediated blockade of the programmed cell death protein 1 (PD-1) inhibitory pathway, which prevents PD-1-mediated immunosuppressive signaling in T cells and can restore effector functions to anergic tumor-infiltrating T cells (2). PD-1/PD-ligand 1 (PD-L1) axis blockade has shown long-term durable

responses in a wide range of cancers, but their efficacy is limited to 10% to 30% of patients (3). Another immunotherapeutic approach involves the stimulation of costimulatory receptors, such as 4-1BB, with agonistic mAbs (4). 4-1BB, also known as CD137, is a member of the TNF receptor (TNFR) superfamily which can be induced on a variety of leukocyte subsets. 4-1BB is a type I single-pass transmembrane receptor with four extracellular cysteine-rich domains (CRD) and an intracellular signaling domain (5). On T cells, 4-1BB is expressed following activation through the T-cell receptor (TCR).

¹Department of Antibody Engineering, Leadartis SL, Madrid, Spain. ²Immunotherapy and Cell Engineering Laboratory, Department of Engineering, Aarhus University, Aarhus, Denmark. ³Cancer Immunotherapy Unit (UNICA), Department of Immunology, Hospital 12 de Octubre, Madrid, Spain. ⁴Immuno-Oncology and Immunotherapy Group, Instituto de Investigación Sanitaria 12 de Octubre (imas12), Madrid, Spain. ⁵Molecular Immunology Unit, Hospital Universitario Puerta de Hierro Majadahonda, Majadahonda, Madrid, Spain. ⁶Biomedical Applications and Pharmacokinetics Unit, Centro de investigaciones Energéticas, Medioambientales y Tecnológicas (CIEMAT), Madrid, Spain. ⁷H120-CNIO Lung Cancer Clinical Research Unit, Instituto de Investigación Sanitaria 12 de Octubre (imas12), and Centro Nacional de Investigaciones Oncológicas (CNIO), Madrid, Spain. ⁸Centro de Investigación Biomédica en Red en Oncología (CIBERONC), Madrid, Spain. ⁹Department of Pathology, Hospital Universitario 12 de Octubre, Madrid, Spain. ¹⁰Department of Pathology, Universidad Complutense, Madrid, Spain. ¹¹Department of Immunology and Immunotherapy, Center for Applied Medical Research (CIMA), University of Navarra, Pamplona, Spain. ¹²Structural Biology Unit, CIC bioGUNE, Parque Tecnológico de Bizkaia, Derio, Spain. ¹³Structural and Chemical Biology Department, Centro de Investigaciones Biológicas, CIB-CSIC, Madrid, Spain. ¹⁴Crystallography and Protein Engineering Unit, Structural Biology Programme, Centro Nacional de Investigaciones

Oncológicas (CNIO), Madrid, Spain. ¹⁵Department of Immunology, University Clinic, University of Navarra, Pamplona, Spain. ¹⁶Instituto de Investigación Sanitaria de Navarra (IdISNA), Pamplona, Spain. ¹⁷Cutaneous Oncology Group, Instituto de Investigación Sanitaria 12 de Octubre (imas12), Madrid, Spain. ¹⁸Department of Medical Oncology, Hospital Universitario 12 de Octubre, Madrid, Spain. ¹⁹Department of Medicine, Universidad Complutense, Madrid, Spain.

Note: Supplementary data for this article are available at Clinical Cancer Research Online (<http://clincancerres.aacrjournals.org/>).

Current address for E.M. Garrido-Martin: Department of Cell Biology and Pharmacogenomics, PharmaMar S.A, Madrid, Spain.

Corresponding Author: Luis Alvarez-Vallina, Cancer Immunotherapy Unit, Hospital Universitario 12 De Octubre, Madrid 28041, Spain. Phone: 349-1779-2773; E-mail: lav.imas12@h12o.es

Clin Cancer Res 2021;27:3167-77

doi: 10.1158/1078-0432.CCR-20-4625

©2021 American Association for Cancer Research.

Translational Relevance

Despite their efficacy in preclinical studies, full-length 4-1BB-agonistic IgGs have not advanced in clinical development due to their severe hepatotoxicity. In this study, we provide preclinical proof of concept for a humanized Fc-free tumor-specific 4-1BB-agonistic trimerbody demonstrating antitumor activity against a wide range of human tumors in humanized immunoavatar mice, as well as synergy with immune checkpoint blockers (ICB). This approach which may provide a way to elicit responses in most patients with cancer while avoiding Fc-mediated adverse reactions. These findings demonstrate that EGFR is an effective target for the development of a broadly applicable tumor-specific 4-1BB-mediated immunotherapy, and support the development of the Trimerbody-EGFR \times 4-1BB as a clinical candidate for treatment of advanced solid tumors.

Binding of its natural ligand [4-1BB-ligand (4-1BBL), TNFSF9] or agonistic mAbs enhances T-cell proliferation and effector functions (6–8), prevents T-cell exhaustion (8), protects from programmed cell death (9, 10), and promotes memory cell differentiation, which may support persistence of tumor-specific T cells (11). Anti-4-1BB-agonistic mAbs have been explored in preclinical cancer models and shown to promote rejection of a range of poorly immunogenic tumors (12–14). However, off-tumor toxicity have been the major impediment to the clinical development of full-length anti-human 4-1BB (anti-hu4-1BB)-agonistic IgGs, and several studies suggest that the toxicity is mainly dependent on Fc–Fc γ R interactions (15–17). The anti-hu4-1BB human IgG₄ urelumab (BMS-663513) caused dose-dependent liver toxicity and was implicated in two deaths (18, 19). Subsequent studies revealed that lower doses reduced liver toxicity, but at the cost of efficacy (19). The anti-hu4-1BB human IgG₂ utomilumab (PF-05082566) has an improved safety profile relative to urelumab, but is also a less potent 4-1BB agonist (20).

New strategies are being actively sought to avoid the off-tumor toxicities associated with Fc–Fc γ R interactions while retaining the antitumor activity associated with 4-1BB costimulation. These approaches aim to confine 4-1BB costimulation to the tumor micro-environment and draining lymph nodes. We have recently described Fc-free tumor-specific trimerbodies targeting a tumor-associated antigen (TAA), such as EGFR (15) or carcinoembryonic antigen (CEA; ref. 21), and murine 4-1BB in an agonistic manner. Both trimerbodies were potent costimulators *in vitro* and the EGFR-targeted 4-1BB-agonistic trimerbody showed enhanced tumor penetration and powerful antitumor activity in immunocompetent mice, while alleviating the systemic cytokine production and T-cell-mediated liver toxicities that are associated with IgG-based 4-1BB agonists (15). More recently, we showed in a liver-specific human EGFR-transgenic immunocompetent mouse that systemic administration of anti-4-1BB-agonistic IgGs resulted in nonspecific immune stimulation and hepatotoxicity, whereas in mice treated with the Fc-free EGFR-specific 4-1BB-agonistic trimerbody no such immune-related adverse effects were observed (22).

Here, we generated and characterized a humanized EGFR-targeted 4-1BB-agonistic trimerbody (4-1BB^{N/C}EGFR), consisting of three anti-hu4-1BB single-chain antibody fragments (scFv) and three anti-human EGFR (huEGFR) single-domain antibodies (V_HH). The humanized 4-1BB^{N/C}EGFR is structurally similar to that of the mouse trimerbody (15), costimulates human T cells *in vitro* in the presence of

huEGFR, and delayed the progression of an EGFR⁺ human colorectal cancer and triple-negative breast cancer (TNBC) cell line-derived xenografts (CLDX) and a patient-derived xenograft (PDX) of EGFR⁺ non-small cell lung cancer (NSCLC), as monotherapy in immune-reconstituted mice. Furthermore, the combination of 4-1BB^{N/C}EGFR with the ICB atezolizumab significantly improved the antitumor immune response, with a near-complete inhibition of tumor growth in humanized mice bearing aggressive EGFR⁺ PD-L1⁺ human TNBC CLDX.

Materials and Methods

Mice

NOD.Cg-Prkdc^{SCID}IL2rg^{tm1Wjl}/SzJ (NSG) female mice were supplied by Charles River Laboratories, Hsd:athymic Nude-Foxn1tm female mice were supplied by Envigo RMS SPAIN S.L., and 129S4-Rag2tm1.1Flv Il2rgtm1.1Flv/J (Rag2^{-/-} IL2R γ null) female mice were bred in the animal facility of CIMA. Animals were maintained under specific-pathogen-free condition with daily cycles of 12 hours light/12 hours darkness, and sterilized water and food were available *ad libitum*. All animal procedures conformed to European Union Directive 86/609/EEC and Recommendation 2007/526/EC, enforced in Spanish law under RD 1201/2005. Animal protocols were approved by the respective Ethics Committee of Animal Experimentation of the participant institutions (IDIPHISA, imas12, CIEMAT and CIMA); they were performed in strict adherence to the guidelines stated in the International Guiding Principles for Biomedical Research Involving Animals, established by the Council for International Organizations of Medical Sciences. The experimental study protocols were additionally approved by local government (PROEX 094/15, 108/15, 076/19, and 166/19).

Antibodies and cell lines

Commercially available antibodies used in the experiments are listed in Supplementary Table S1. Recombinantly produced antibodies are listed in Supplementary Table S2. HEK293 (CRL-1573), MDA-MB-231 (HTB-26), A431 (CRL-1555), NIH/3T3 (CRL-1658), and CHO-K1 (CCL-61) cells were obtained from the ATCC and cultured in DMEM (Lonza) supplemented with 2 mmol/L L-glutamine, 10% (vol/vol) heat-inactivated FCS (Merck Life Science), and antibiotics (100 units/mL penicillin, 100 mg/mL streptomycin; all from Life Technologies) referred as to DMEM complete medium (DCM), at 37°C in 5% CO₂ humidity. NIH/3T3 cells expressing huEGFR (3T3^{huEGFR}; ref. 23) were kindly provided by A. Villalobo (IIBm). The hu4-1BB-expressing HEK293 cell line (HEK293^{hu4-1BB}) was generated by transfection with the expression vector pCMV3-Flag-TNFRSF9 (SinoBiological) and selected in DCM with 500 μ g/mL G418 (Life Technologies). CHO-K1 Cells expressing human Fc γ RIIb (CD32) were from Promega (No. JA2251). All cell lines were used within 3 months of thawing and checked for *Mycoplasma* using PCR every month using the Mycoplasma Plus TM Primer Set (Biotools B&M Labs).

Construction of expression vectors

To generate the SAP3.28 scFv-based N-terminal trimerbody, the DNA fragments encoding the FLAG-strep II-SAP3.28^{HL} (V_H-linker-V_L) scFv was synthesized by Geneart AG and subcloned as *Hind*III/*Not*I into the expression vector pCR3.1-MFE23^N (24) resulting in pCR3.1-FLAG-strepII-SAP3.28^{HL-N}-myc/His. The C-terminal myc/His tag-sequence was removed by PCR from the plasmids with Fw-CMV and Stop-*Xba*I-Rev primers (Supplementary Table S3). The

Flag-strep II-SAP3.28^{HL} scFv gene was subcloned as *HindIII/NotI* into a vector containing the human collagen XVIII-derived homotrimerization (TIE^{XVIII}) domain and the anti-human EGFR single-domain antibody (V_{HH}; EGa1; ref. 25), resulting in the bispecific trimerbody-expressing vector pCR3.1-FLAG-strepII-SAP3.28^{HL-N18/C18}EGa1. All the sequences were verified using primers FwCMV and RvBGH (Supplementary Table S3).

In vitro 4-1BB-dependent NFκB activation assay

4-1BB-dependent activation of activated NFκB assay was performed on thaw-and-use GloResponseNFκB-*luc2/4*-1BB Jurkat cells (Promega, No. JA2351) according to the manufacturer's instructions (Supplementary Materials and Methods).

Human PBMC and T-cell activation assays

Human PBMCs or isolated T cells (Supplementary Materials and Methods; 1.5×10^5 cells/well) were plated in triplicate in flat bottom 96-well plates, in RPMI supplemented with 10% FCS and 50 μmol/L β-mercaptoethanol (Life Technologies) and cocultured with 45 Gy irradiated target cells (3T3 or 3T3^{hEGFR}) at an effector/target ratio of 5:1. The anti-hu4-1BB agonists antibodies and controls were added at 10-fold serial dilutions in the presence of anti-huCD3 (OKT3) mAb at 0.05 μg/mL. After 72 hours, cell-free supernatants were analyzed by ELISA for cytokine secretion. Irradiated EGFR⁺PD-L1⁻ cells (3T3^{hEGFR}) or EGFR⁺PD-L1⁺ cells (MDA-MB-231; 3×10^4 cells/well) were seeded with huPBMCs (1.5×10^5 cells/well), activated with anti-huCD3 at 0.05 μg/mL, in the presence of anti-PD-L1 (atezolizumab) alone (10 μg/mL) or combined with 4-1BB^{N/C}EGFR (1 μg/mL). Cell-free supernatants were measured for IFNγ after 72 hours by ELISA (Diaclone, No. 851560005).

Humanized colorectal cancer CLDX models

HT29 cells (1×10^6) were implanted subcutaneously into the dorsal space of 6-week-old Rag2^{-/-} IL2Rγ null female mice, followed by the intraperitoneal infusion of freshly huPBMCs (1×10^7 cells/mouse). Tumor growth was monitored by caliper measurements three times a week, and when tumors reached approximately 0.4 cm in diameter, mice were randomized to receive treatment ($n = 7-8$ /group). Measurements were conducted in a random order by the investigator who was blinded to the treatment assignment. Mice were treated every 3 days with five intraperitoneal injections of CEA^N or 4-1BB^{N/C}EGFR trimerbodies (4 mg/kg) or every week with three intraperitoneal injections of 4-1BB IgG (4 mg/kg). MDA-MB-231 cells (2×10^6) were resuspended in PBS and mixed with matrigel (30%). Cells were implanted subcutaneously on right dorsal flank of 6-week-old NSG female mice, followed by an intraperitoneal injection of freshly isolated huPBMCs (1×10^7 cells/mouse). Tumor growth was monitored by caliper measurements three times a week. Tumor-bearing mice (0.2 cm diameter) were randomly divided into four groups ($n = 5-6$ /group) and the investigator was blinded for treatment allocation. Mice were treated every three days with five intraperitoneal injections of 4-1BB^{N/C}EGFR trimerbodies (4 mg/kg), or every week with three intraperitoneal injections of PD-L1 IgG (4 mg/kg), alone or in combination. Mice weights were measured twice a week to monitor toxicity. Mice were euthanized at any sign of distress and/or due to 10% to 15% of weight loss.

Humanized PDX model

For this study, the previously amplified lung PDX TP103 was selected according to its histologic type, genetic background (*EGFR* and *TP53* mutated), and huEGFR cell surface expression (26). Tumors

were cut into ≈ 50 -mm³ pieces, and implanted subcutaneously through a tiny incision into the dorsal space of anesthetized 6-week-old NSG female mice. Tumor growth was monitored by caliper measurements every 3 to 4 days, and when tumors reached approximately 0.5 cm in diameter, mice were randomized into groups ($n = 6-7$ /group) with similar mean tumor sizes and SDs, and freshly isolated huPBMCs (1×10^7 cells/mouse) from healthy donors were intraperitoneally infused. Mice were treated every 3 days with five intraperitoneal injections of 4-1BB^{N/C}EGFR (4 mg/kg). Mice weights were measured once a week to monitor toxicity. Mice were euthanized when the weight loss was $\geq 10\%$ to 15%, when tumor size reached a diameter of 1.0 cm any dimension, when tumors ulcerated, or at any sign of mouse distress.

Statistical analysis

Statistical analysis was performed using GraphPad Prism Software version 6.0. In general, the *in vitro* experiments were done in triplicates and values are presented as mean \pm SD from one of at least three separate experiments. Significant differences (*P* value) were discriminated by applying a two-tailed, unpaired Student *t* test assuming a normal distribution. *P* values are indicated in the corresponding figures for each experiment. EC₅₀ were calculated using a nonlinear regression curve (log agonist vs. normalized response-variable response). Mean tumor volume are presented for each group using a scatter plot as mean \pm SD. To assess the differences between treatment groups, *P* values were determined by one-way ANOVA adjusted by the Bonferroni correction for multiple comparison tests.

Results

Generation and characterization of 4-1BB-agonistic humanized trimerbodies

Anti-hu4-1BB trimerbodies were generated using scFv-encoding genes derived from the anti-hu4-1BB-agonistic SAP3.28 mAb (Supplementary Fig. S1A), which binds to hu4-1BB CRD-1 (27). The SAP3.28 IgG (hereafter referred to as 4-1BB IgG) is a chimeric molecule displaying a humanized V_L domain and a partially humanized V_H domain that preserves the murine FR3 region to retain antigen binding, and the Fc region of murine IgG₁ (27). Like urelumab, which recognizes the N-terminus of CRD-1 (28), 4-1BB IgG does not block the hu4-1BB receptor/hu4-1BBL interaction (Supplementary Fig. S2A–S2C). Furthermore, we showed that the epitopes of 4-1BB IgG and urelumab do not overlap (Supplementary Fig. S2D and S2E). We designed a SAP3.28 scFv-based anti-hu4-1BB N-terminal trimerbody (4-1BB^N) by fusing the SAP3.28 scFv to the human collagen XVIII-derived homotrimerization (TIE^{XVIII}) domain by a flexible linker (Supplementary Fig. S1B and S1C), and a bispecific trimerbody by fusing the anti-EGFR EGa1 V_{HH} antibody (25) to the C-terminus of the 4-1BB^N to generate the construct called 4-1BB^{N/C}EGFR (Fig. 1A). Both trimerbodies were purified from conditioned medium from stably transfected HEK293 cells by Strep-Tactin affinity chromatography, with proteins yields (3.5 and 4.5 mg/L, respectively) that were $> 95\%$ pure (Supplementary Fig. S3A). Mass spectrometry (using MALDI-TOF, not shown) confirmed the absence of the signal sequences in the purified antibodies. SEC-MALS experiments on both 4-1BB^N and 4-1BB^{N/C}EGFR yielded major peaks with molar masses of 111 and 160 kDa, respectively (Supplementary Fig. S3B and S3C), which are consistent with trimeric molecules. Minor peaks at smaller volumes with molar masses of 217 and 340 kDa indicate the presence of dimers of trimers, as previously observed for other trimerbodies (15). Circular dichroism measurements show predominant b-sheet

structures and cooperative thermal denaturations ($T_m \approx 60^\circ\text{C}$; Supplementary Fig. S3D and S3E). Small angle X-ray scattering (SAXS) was used to study the three-dimensional structure of both trimerbodies. The 4-1BB^N trimerbody shows a flat distribution, with a well-defined TIE^{XVIII} core in the center and the scFvs partially extended on the same plane, like the spokes on a wheel (Supplementary Figs. S4 and S5; Supplementary Table S4) The 4-1BB^{N/C}EGFR trimerbody maintains the same planar configuration of 4-1BB^N with its additional small-sized EGFR V_{HH} domains interspersed between the 4-1BB scFvs to resemble a six-bladed ninja star (Fig. 1B; Supplementary Fig. S5; Supplementary Table S4).

Biolayer interferometry (BLI) was used to measure the association and dissociation kinetics of 4-1BB^N and 4-1BB^{N/C}EGFR binding to hu4-1BB, and of 4-1BB^{N/C}EGFR and the anti-EGFR ATTACK antibody (29) binding to huEGFR (Fig. 1C). The bispecific ATTACK antibody is an evolution of the tandem trimerbody format (30) which combines three EGFR-binding V_{HH} antibodies with a single CD3-binding scFv (29). All interactions were of high affinity (with low picomolar K_D values), indicating functional trivalence of the trimer-

bodies toward the antigens displayed on a biosensor surface (Supplementary Table S5). The kinetics of huEGFR binding by these trivalent antibodies is consistent with previous studies (15, 29). In a complementary experiment, 4-1BB^N and the 4-1BB^{N/C}EGFR were first loaded onto hu4-1BB immobilized on the surface of biosensors, which were then transferred into buffer containing huEGFR. 4-1BB^{N/C}EGFR, but not 4-1BB^N, was able to bind soluble huEGFR while remaining bound to the immobilized hu4-1BB, further confirming its bivalence and its capability to bind both antigens simultaneously (Fig. 1D). Furthermore, 4-1BB^{N/C}EGFR bound to mouse (mo-), cynomolgus (cy-) and huEGFR, as well as to cy4-1BB and hu4-1BB, but to a much lower extent to mo4-1BB (Supplementary Fig. S6A and S6B). Their ability to detect hu4-1BB and huEGFR in a cellular context was analyzed by flow cytometry. The 4-1BB^{N/C}EGFR trimerbody bound to wild-type HEK293 (EGFR⁺) cells, to HEK293 cells transfected to express hu4-1BB on their cell surface (HEK293^{hu4-1BB}), and to mouse 3T3 cells expressing huEGFR (3T3^{huEGFR}) but not to wild-type 3T3 cells (Supplementary Fig. S7). In contrast, the 4-1BB IgG only bound HEK293^{hu4-1BB} cells. To further assess the multivalent binding of

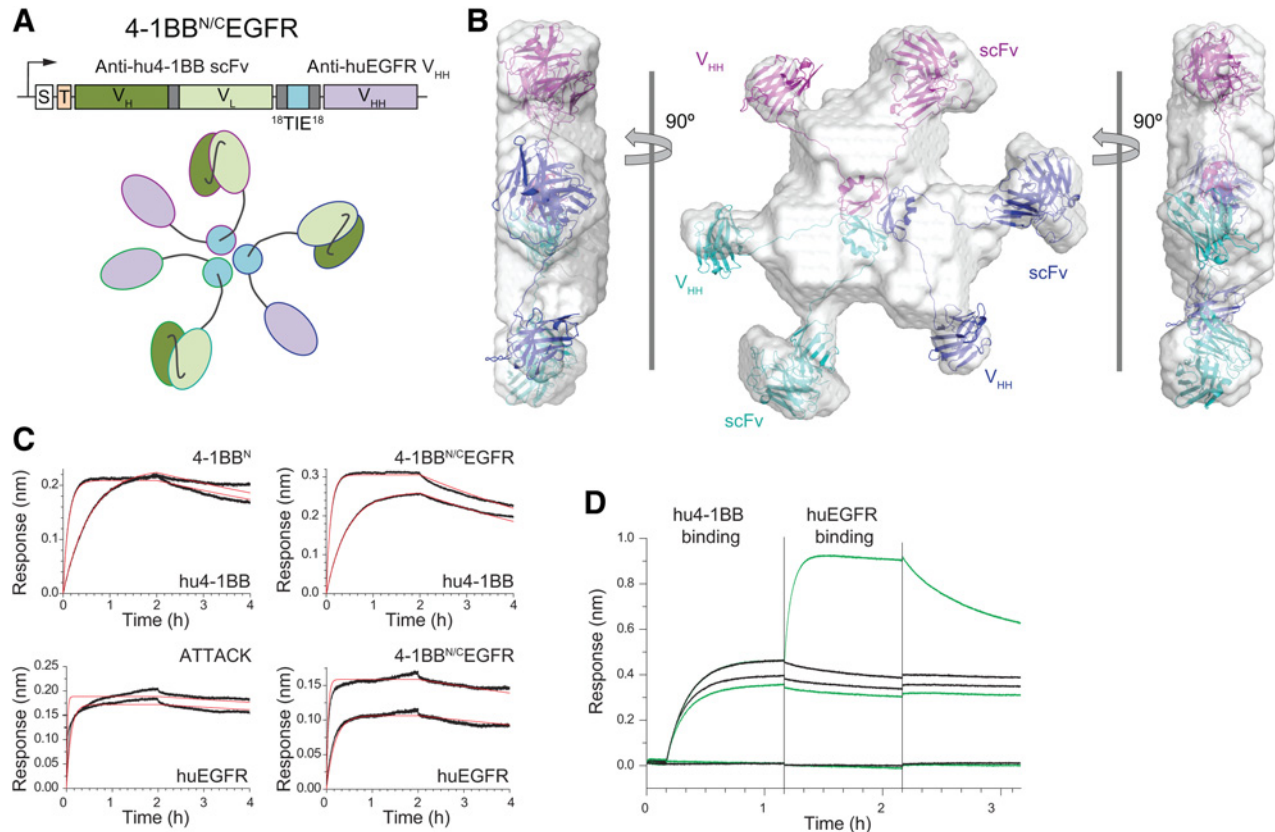


Figure 1.

Design and characterization of the humanized Fc-free tumor-targeted 4-1BB-agonistic trimerbody (4-1BB^{N/C}EGFR). **A**, Schematic diagrams showing the gene layout and domain structure, and arrangement of 4-1BB^{N/C}EGFR in solution, as determined by SAXS. **B**, Rigid-body fitting of the model corresponding to 4-1BB^{N/C}EGFR inside the SAXS envelope (colored in pale gray). Each chain has been colored in blue, magenta, and cyan. **C**, Experimental sensorgrams (black lines) and calculated (red lines) obtained from BLI showing the interactions between 4-1BB^N and 4-1BB^{N/C}EGFR trimerbodies (at 1 and 5 nmol/L concentrations) and immobilized hu4-1BB (top), and those between anti-huEGFR ATTACK and 4-1BB^{N/C}EGFR trimerbody (at 1 and 5 nmol/L concentrations) and immobilized huEGFR (bottom). The kinetic rate constants used for the calculated curves are given in Supplementary Table S5. **D**, Simultaneous binding to both immobilized hu4-1BB and huEGFR in solution was demonstrated for 4-1BB^{N/C}EGFR (green) but not 4-1BB^N (black); 5 nmol/L of either trimerbody first bound to immobilized hu4-1BB, after which the biosensors were moved into 10 nmol/L huEGFR.

4-1BB^{N/C}EGFR, we studied its capacity to inhibit proliferation and EGFR phosphorylation in A431 cells (25). Both 4-1BB^{N/C}EGFR and cetuximab, an EGF-competitive inhibitor (31), but neither the anti-human CD20 rituximab nor the parental 4-1BB IgG, inhibited A431 proliferation, in a dose-dependent manner ($P = 0.003$ and $P = 0.0005$, respectively, for the higher doses of both antibodies, vs. equimolar doses of control antibodies), as well as EGFR phosphorylation (Supplementary Fig. S8A and S8B).

The Fc-free EGFR-targeted 4-1BB-agonistic humanized trimerbody significantly enhances T-cell costimulation in the presence of EGFR-expressing cells

The agonist activities of the three SAP3.28-derived antibodies and urelumab were assessed using NFκB-*luc2/4*-1BB Jurkat cells (Jurkat^{NFκB}) that constitutively express hu4-1BB on the cell surface and a luciferase reporter driven by a NFκB response element. Jurkat^{NFκB} reporter cells were cocultured with target cells stably expressing either huFcγRIIb (CHO^{huFcγRIIb}) or huEGFR (3T3^{huEGFR}), as well as nontransfected CHO or 3T3 cells as negative controls; the expression of cell surface huFcγRIIb and huEGFR were demonstrated by flow cytometry (Fig. 2A and B). Titrations of bivalent (4-1BB IgG or urelumab), or trivalent (4-1BB^N or 4-1BB^{N/C}EGFR) anti-hu4-1BB antibodies were then added to the cocultured cells. In the absence of Fc- or EGFR-mediated antibody cross-linking at the target cell surface (i.e., in cocultures with nontransfected CHO or 3T3 cells), 4-1BB IgG showed little to no induction over untreated Jurkat^{NFκB} cells at all tested concentrations, both anti-hu4-1BB trimerbodies showed an approximately 10-fold induction, and urelumab showed an approximately 20-fold induction (Fig. 2C and D). In the presence of FcγRIIb-mediated cross-linking (i.e., using CHO^{huFcγRIIb} as target cells), 4-1BB IgG induced a NFκB dose-dependent activation with a 26-fold induction ($P = 0.0008$) and urelumab's induction was further increased to 40-fold ($P = 0.003$; Fig. 2C). Neither trimerbody showed a FcγRIIb-mediated increase in induction (Fig. 2C). The trimerbody-mediated 4-1BB signaling was significantly strengthened when target cells expressed huEGFR ($P = 0.0008$), leading to a 40-fold increase of NFκB luciferase reporter activity (Fig. 2D). Induction by 4-1BB IgG, urelumab, and 4-1BB^N was not affected by huEGFR expression (Fig. 2D). The negative control antibodies moIgG1, huIgG4, and CEA^N, a trimerbody recognizing CEA, showed no activation (Supplementary Fig. S9A and S9B). We then used huPBMCs or T cells from healthy donors to investigate the effect of the anti-hu4-1BB antibodies on IFNγ secretion when cocultured with irradiated 3T3 or 3T3^{huEGFR} cells, both with and without a suboptimal dose of anti-huCD3 mAb. The 4-1BB^{N/C}EGFR trimerbody had a dose-dependent activating effect on IFNγ secretion only when huPBMCs or T cells were cocultured with EGFR⁺ cells; no induction was observed with EGFR⁻ cells (Fig. 2E and F). Under these conditions, the effect of 4-1BB IgG and CEA^N was minimal and independent of EGFR expression (Fig. 2E; Supplementary Fig. S10). These data show that 4-1BB^{N/C}EGFR induces strong, EGFR-dependent T-cell costimulation and IFNγ secretion that requires initial signaling through the TCR/CD3 complex (signal 1). Subsequently, huPBMCs were cocultured with irradiated EGFR⁺PD-L1⁻ (3T3^{huEGFR}) or EGFR⁺PD-L1⁺ (MDA-MB-231) cells (Fig. 2G) in the presence of 4-1BB^{N/C}EGFR and the PD-L1-blocking antibody atezolizumab. When combined with a suboptimal dose of anti-huCD3 mAb, the 4-1BB^{N/C}EGFR trimerbody significantly enhanced IFNγ secretion ($P = 0.0007$ 3T3^{huEGFR} cells; $P = 0.0002$ MDA-MB-231 cells; Fig. 2H). The addition of atezolizumab significantly increased IFNγ

levels when huPBMCs were cocultured with MDA-MB-231 cells in the presence of 4-1BB^{N/C}EGFR ($P = 0.02$; Fig. 2H).

Pharmacokinetics of⁸⁹Zr-labeled 4-1BB^{N/C}EGFR trimerbody

The 4-1BB^{N/C}EGFR trimerbody retained close to 100% of its initial binding activity after 4 days in human serum at 37°C (Supplementary Fig. S11A and S11B). Chelation with p-SCN-Bn-Deferoxamine (Df) of the 4-1BB^{N/C}EGFR trimerbody did not alter its SDS-PAGE migration pattern nor compromise its binding activity (Supplementary Fig. S12A and S12B). After radiolabeling, the RCY (radiolabeling yield) and RQP (radiochemical purity) of purified [⁸⁹Zr]Zr-Df-4-1BB^{N/C}EGFR were 40% and 95%, respectively. The AIC values were 10.97 and -22.66 for one and two compartment of [⁸⁹Zr]Zr-Df-4-1BB^{N/C}EGFR, respectively; thus, the disposition of the 4-1BB^{N/C}EGFR trimerbody was better explained through a bicompartamental model (Supplementary Table S6). After intravenous administration, the elimination of [⁸⁹Zr]Zr-Df-4-1BB^{N/C}EGFR was biphasic, with a half-time of 7.3 hours for the rapid distribution phase and 66.8 hours for the slow distribution phase (Fig. 3A). The volume of distribution at steady state was 66.5 mL (2.63 L/kg) and the plasma clearance 0.97 mL/hour (37.6 mL/kg/hour). As the blood-to-plasma ratio was 0.62, the blood clearance value obtained was very low (0.062 L/kg/hour) compared with the cardiac output (21.7 L/kg/hour in mouse), which is generally desirable for developing a drug with a low dosage regimen (32).

Antitumor activity of the Fc-free EGFR-targeted 4-1BB-agonistic humanized trimerbody

We tested the 4-1BB^{N/C}EGFR trimerbody for antitumor activity in huPBMC-driven humanized immunoavatar mouse models. Rag2^{-/-}IL2Rγ^{null} mice were intraperitoneally injected with huPBMCs and then human HT-29 colorectal cancer cells were subcutaneously inoculated (Fig. 3B). Transferred human T cells become activated and develop pathogenic xeno-reactivity, a process called xenograft-versus-host disease (xGVHD; ref. 33), which is a valuable model for testing immunomodulatory strategies, where the engrafted human T cells are amenable for modulation by therapeutic agents (34–36). When tumors reached approximately 0.4 cm in diameter, mice were treated with five trimerbody (CEA^N or 4-1BB^{N/C}EGFR) intraperitoneal injections at 3/4-day intervals, or three weekly equimolar doses of 4-1BB IgG, as depicted in Fig. 3B. The dose and treatment schedule was designed in a similar way to what was conducted with the anti-mo4-1BB agonists in an immunocompetent model of colorectal cancer (15). The 4-1BB^{N/C}EGFR-treated group showed a significantly slower tumor growth compared with the untreated group ($P = 0.01$), and the CEA^N-treated groups ($P = 0.004$; Fig. 3C). Notably, the humanized 4-1BB^{N/C}EGFR trimerbody provided antitumor activity *in vivo* comparable with the 4-1BB IgG (Fig. 3C).

We next sought to determine whether the antitumor effect would also occur in an EGFR⁺ NSCLC PDX-bearing huPBMC-driven humanized NSG mice model (TP103; Fig. 3D and E). As shown in Fig. 3F, the 4-1BB^{N/C}EGFR-treated mice showed a reduced tumor growth compared with the control group. The improved tumor growth control was accompanied of significant changes in the tumor-infiltrating lymphocyte (TIL) infiltration pattern. In both groups, a diffuse infiltration of CD3⁺ T lymphocytes surrounding and involving tumor cell nests was detected (Supplementary Fig. S13). In the PBS-treated mice, there was a prevalence of CD4⁺ T cells with a CD4/CD8 ratio of 2.8 (Fig. 3G–I). In the 4-1BB^{N/C}EGFR-treated group, a significant increase in the number of CD8⁺ T cells ($P = 0.04$) was observed, accompanied by a reduction in the number of Foxp3⁺ cells ($P = 0.01$; Fig. 3G–I; Supplementary Fig. S13).

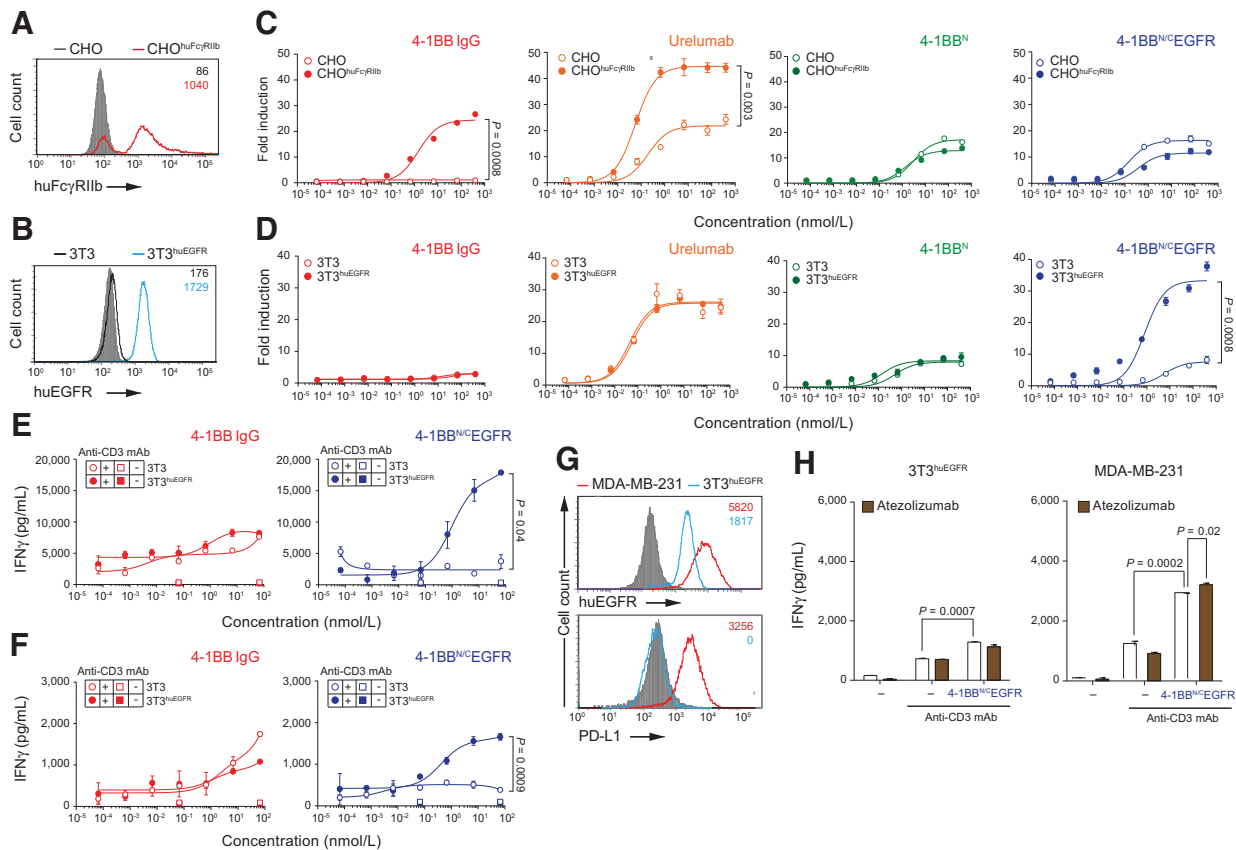


Figure 2.

The 4-1BB^{N/C}EGFR trimerbody significantly enhances *in vitro* T-cell costimulation in the presence of huEGFR-expressing cells and signal 1. Flow cytometry analysis of huFc γ RIIb (CD32) expression in CHO and CHO^{huFc γ RIIb} cells (A), and of huEGFR expression in 3T3 and 3T3^{huEGFR} cells (B). Cells incubated with PE-conjugated isotype control mAb are shown as gray-filled histogram. Fluorescence intensity (abscissa) is plotted against relative cell number (ordinate). The numbers indicate the mean fluorescence intensity. Jurkat^{hu4-1BB} cells were cocultured with CHO or CHO^{huFc γ RIIb} cells (C) and 3T3 or 3T3^{huEGFR} cells (D) in the presence of 10-fold increasing concentrations of 4-1BB IgG, urelumab, 4-1BB^N or 4-1BB^{N/C}EGFR antibodies, and after 6 hours at 37°C luminescence determined. Data were presented as fold induction relative to the values obtained from unstimulated Jurkat^{hu4-1BB} cells. Representative dose-concentration curves are presented and expressed as a mean \pm SD ($n = 3$). Significance was determined by unpaired Student *t* test. Human PBMCs (E) and T cells (F; 1.5×10^5 /well) isolated from healthy donors were cocultured with irradiated 3T3 or 3T3^{huEGFR} cells at an E:T ratio of 5:1. The anti-hu4-1BB agonists antibodies (4-1BB IgG or 4-1BB^{N/C}EGFR) and controls were added at 10-fold serial dilutions in the presence or absence of anti-huCD3 mAb (0.05 μ g/mL), and IFN γ secretion was analyzed after 72 hours (mean \pm SD, $n = 3$). Significance was determined by unpaired Student *t* test. G, Flow cytometry analysis of huEGFR expression (top) or huPD-L1 expression (bottom) in 3T3^{huEGFR} and MDA-MB-231 cells. Cells incubated with phycoerythrin-conjugated isotype control mAbs are shown as gray-filled histogram. H, Irradiated EGFR⁺PD-L1⁻ cells (3T3^{huEGFR}) or EGFR⁺PD-L1⁺ cells (MDA-MB-231; 3×10^4 cells/well) were cocultured with huPBMCs at a 5:1 E:T ratio, activated with anti-huCD3 mAb (0.05 μ g/mL), in the presence of anti-PD-L1 alone or combined with 4-1BB^{N/C}EGFR. Cell-free supernatants were measured for IFN γ after 72 hours by ELISA. Data are presented as mean \pm SD ($n = 3$). Significance was calculated by an unpaired Student *t* test. One representative experiment out of three independent experiments were shown (A and C). If primary cells were used, then at least three different donors were tested.

We compared the toxicity profile in huPBMC-driven humanized NSG mice treated with 4-1BB IgG or 4-1BB^{N/C}EGFR trimerbody (6 mg/kg) once a week for 3 weeks and euthanized 1 week later. The histologic study of the livers revealed that 4-1BB IgG treatment exacerbated xGVHD. Details of the liver infiltration in a representative mouse of each group of treatment are depicted in Fig. 3J, showing extensive perivascular mononuclear cell infiltration in the group treated with the IgG-based 4-1BB agonist. We then studied the concentrations of human IFN γ in serum samples collected at sacrifice. 4-1BB IgG treatment significantly increase IFN γ levels over 4-1BB^{N/C}EGFR treatment ($P = 0.001$), where the levels were comparable with PBS-treated animals (Fig. 3K).

The combination of 4-1BB^{N/C}EGFR and atezolizumab induces tumor regression

The therapeutic potential of combining 4-1BB^{N/C}EGFR with the PD-L1 blocker atezolizumab was investigated in huPBMC-driven humanized NSG mice bearing human EGFR⁺PD-L1⁺ MDA-MB-231 (Fig. 2G) TNBC xenografts (Fig. 4A). Atezolizumab monotherapy was able to reduce tumor growth by approximately 60%, while 4-1BB^{N/C}EGFR monotherapy showed an approximately 90% tumor growth reduction (Fig. 4B). The combination of atezolizumab plus 4-1BB^{N/C}EGFR resulted in an additional decrease in tumor growth (Fig. 4B). In the PBS-treated group, large nests of neoplastic pleomorphic cells with intense cytokeratin (CK) expression with dense lymphocyte infiltration (Fig. 4C and D) were observed.

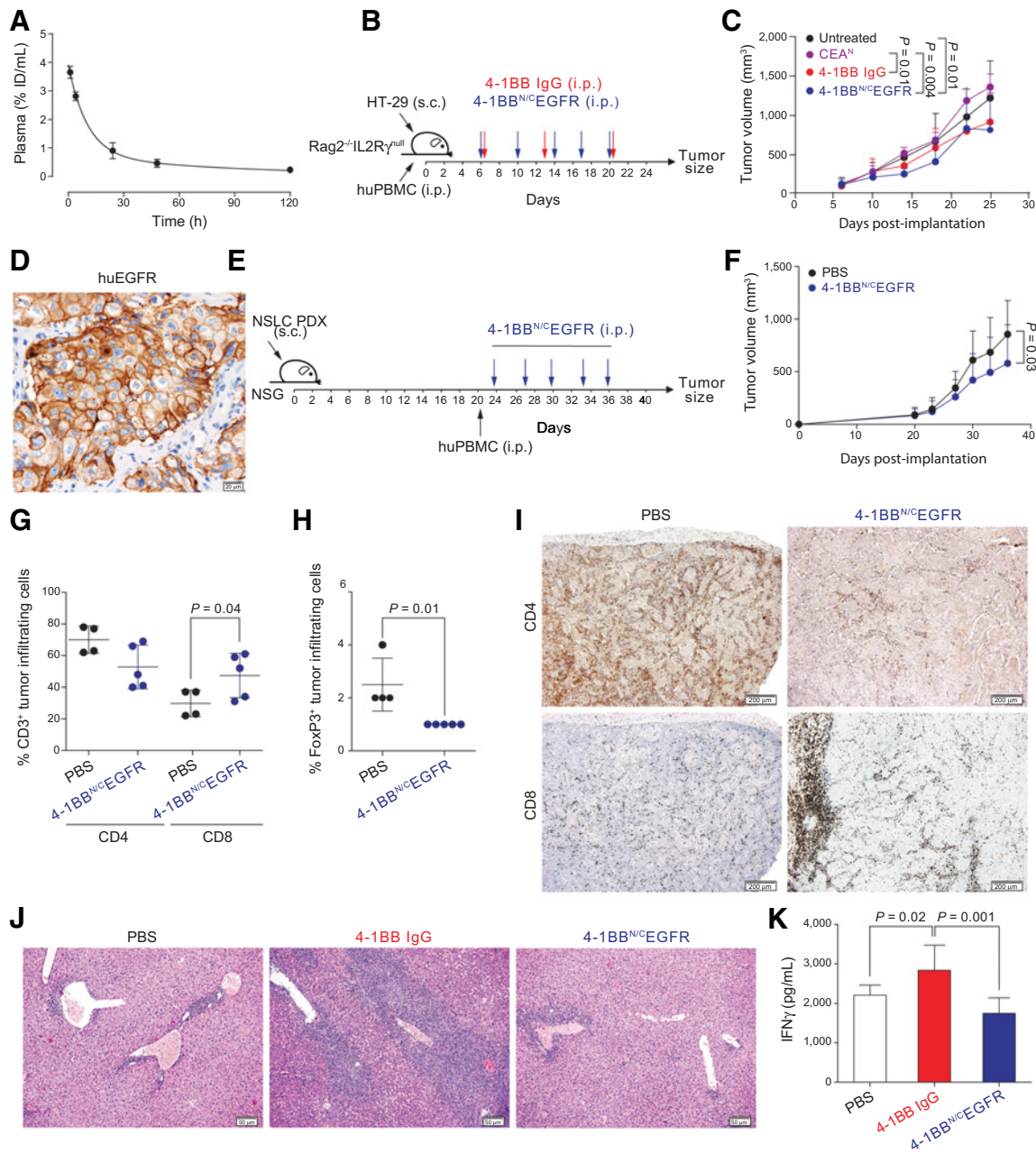


Figure 3.

4-1BB^{N/C}EGFR trimerbody displayed significant tumor growth inhibition in humanized mouse models. **A**, Pharmacokinetic profile expressed as % ID/mL in plasma versus time of ⁸⁹Zr-4-1BB^{N/C}EGFR following intravenous administration. Data are shown as mean ± SD (*n* = 2-6). **B**, Rag2^{-/-}IL2Rγ^{null} mice were inoculated subcutaneously with HT29 tumor cells and intraperitoneally with freshly isolated huPBMCs, and when tumors reached approximately 0.4 cm in diameter randomized into groups (*n* = 7-8/group) with similar mean tumor sizes and SDs, and treated with PBS, five intraperitoneal injections of CEA^N or 4-1BB^{N/C}EGFR trimerbodies (4 mg/kg) or with three intraperitoneal injections of 4-1BB IgG (4 mg/kg). **C**, Average tumor volume growth of mice in each group are represented. Data are presented as the mean ± SD. Significance was determined by one-way ANOVA adjusted by the Bonferroni correction for multiple comparison test. **D**, Analysis of huEGFR expression by IHC in NSCLC PDX TP103. **E**, NSG mice were subcutaneously inoculated with small fragments of previously amplified TP103 and when tumors reached approximately 0.5 cm in diameter randomized into groups (*n* = 6-7/group) with similar mean tumor sizes and SDs, and freshly isolated huPBMCs intraperitoneally injected. Mice were treated with PBS or 4-1BB^{N/C}EGFR. **F**, Average tumor volume growth of mice in each group are represented. Data are presented as the mean ± SD. Significance was determined by an unpaired Student *t* test. In both *in vivo* assays, mice weights were measured once a week to monitor toxicity and animals were euthanized at any sign of distress and/or due to 10% to 15% of weight loss. Percentage of CD4⁺ and CD8⁺ cells (**G**) or FoxP3⁺ cells (**H**) on tissue sections from PBS- and 4-1BB^{N/C}EGFR-treated mice (mean ± SD, *n* = 4-5). Significance was calculated by an unpaired Student *t* test. **I**, Representative IHC staining for CD4 and CD8 is shown. Tumors were taken from the experiment shown in **F** at termination. **J**, Hematoxylin and eosin staining in representative tissue sections of liver of mice treated with PBS, 4-1BB IgG, and 4-1BB^{N/C}EGFR. Scale bars are shown. **K**, Human IFNγ serum levels of mice were studied in week 4 (mean ± SD, *n* = 4). Significance was calculated by an unpaired Student *t* test.

Importantly, the percentage of CK⁺ cells was significantly lower in the 4-1BB^{N/C}EGFR monotherapy group ($P = 0.04$) and in the combination therapy group ($P = 0.0002$) than in atezolizumab monotherapy group (Fig. 4C). With combination therapy, the percentage of CK⁺ cells was at most 30% in 5 of 6 mice and in one mouse, TNBC cells were completely eradicated (Fig. 4E). This reduction in tumor burden was associated with a significantly increased proportion of CD8⁺ T cells in the 4-1BB^{N/C}EGFR-treated groups ($P = 0.03$ and $P = 0.04$; Fig. 4D and E).

Discussion

Immune checkpoint receptors, both coinhibitory and costimulatory, are membrane molecules expressed by immune cells that regulate the activation and effector functions of T cells (37). These regulatory receptors can be manipulated by the exogenous administration of antibodies to enhance preexisting antitumor immunity (38). The blockade of inhibitory checkpoints, such as CTLA-4 and PD-1/PD-L1, with antagonistic mAbs have shown remarkable efficacy in several types

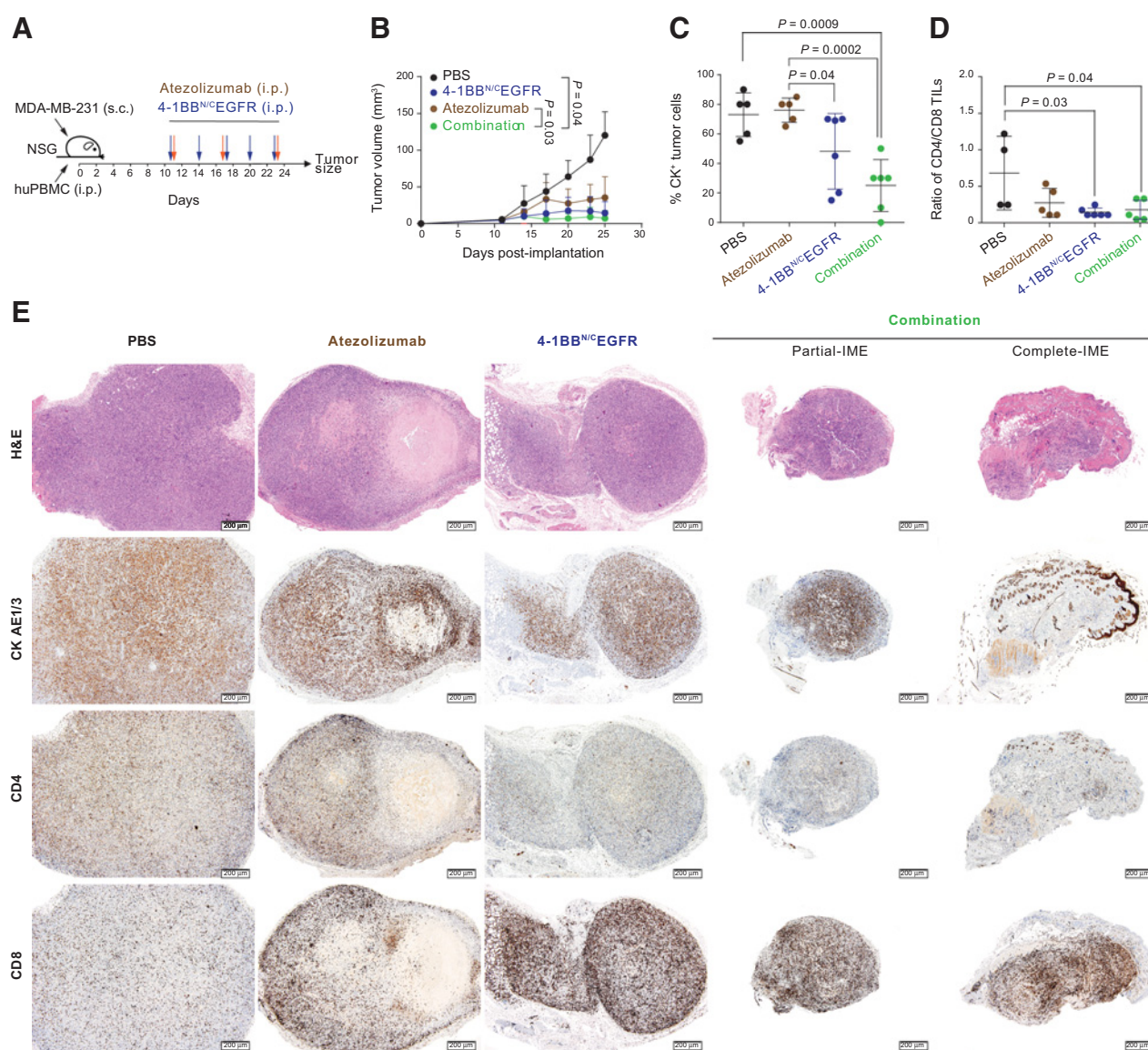


Figure 4.

Combination of 4-1BB^{N/C}EGFR and full-length PD-L1-blocking antibodies induces tumor regression in an humanized MDA-MB-231 TNBC xenograft model. **A**, NSG mice were inoculated subcutaneously with MDA-MB-231 tumor cells and injected intraperitoneally with freshly isolated huPBMCs, and when tumors reached approximately 0.2 cm in diameter randomized into groups ($n = 5-6$ /group), and treated with PBS or 4-1BB^{N/C}EGFR or atezolizumab alone or in combination. **B**, Average tumor volume growth of mice in each group are represented. Data are presented as the mean \pm SD. Mice weights were measured once a week and animals were euthanized at any sign of distress and/or due to 10% to 15% of weight loss. Significance was determined by one-way ANOVA adjusted by the Bonferroni correction for multiple comparison test. Percentage of cytokeratin (CK)⁺ cells (**C**) and CD4/CD8 ratio of TILs (**D**) on tumor sections taken from the experiment shown in **B** at termination. Data are presented as mean \pm SD ($n = 4-6$). Significance was calculated by an unpaired Student *t* test. **E**, Representative low magnification images of hematoxylin and eosin (H&E) and immunohistochemically stained samples for cytokeratin, CD4 and CD8 are shown. In the combination therapy group, two representative specimens are shown, with partial or complete immune-mediated eradication (IME) of TNBC cells.

of cancer, with manageable toxicity profiles; however, their overall response rate remains around 30% (39). Agonistic antibodies targeting costimulatory checkpoints, such as 4-1BB, OX40, CD40, GITR, and ICOS, are able to bias T cells toward an effector outcome and overcome anergy-inducing immunosuppressive signaling in the tumor microenvironment, thus providing strong rationale to be combined with ICB (38). However, despite significant interest and effort, no such antibody has yet received regulatory approval. Among them, anti-4-1BB mAbs have shown robust antitumor activity in preclinical models (12). However, the clinical development of full-length IgG anti-hu4-1BB-agonistic mAbs is facing serious challenges due to low efficacy (utomilumab) or severe hepatotoxicity (urelumab; ref. 18). We recently generated Fc-free tumor-targeted murine 4-1BB-agonistic trimerbodies that induced effective antitumor immunity without liver toxicity in immunocompetent mice (15).

Here, we characterize a Fc-free bispecific humanized trimerbody which binds to human 4-1BB and EGFR. This 4-1BB^{N/C}EGFR trimerbody is efficiently produced and structural studies showed that the trimerbody primarily forms the intended trimeric structure, with protein folding and configuration nearly identical to that of the murine trimerbody (15). The antibody domains are positioned around the human collagen XVIII homotrimerization domain in a hexagonal configuration, and the binding studies provided quantitative evidence for multivalent interactions with both human 4-1BB and EGFR. These results demonstrate the robustness of the trimerbody scaffold to generate functional multivalent and multispecific molecules with a predictable and well-defined structure.

The binding of three TNFRSF receptors to a single trimeric ligand nucleates receptor clustering to induce signaling, but multiple complexes are required for signaling to reach effective levels (40). Anti-4-1BB-agonistic mAbs can be classified as either strong or weak agonists. A strong agonist (e.g., urelumab) can induce signaling activation without FcγR-mediated cross-linking, while a weak agonistic (e.g., utomilumab) requires FcγR-mediated cross-linking to meaningfully induce 4-1BB signaling (41). Here, we demonstrate in a hu4-1BB-reporting cell line that a bivalent (IgG) anti-hu4-1BB antibody derived from the SAP3.28 antibody (27) is dependent on the presence of FcγRIIb to induce 4-1BB signaling and can therefore be classified as weak agonists. However, SAP3.28-derived trimerbodies induce partial 4-1BB signaling even without additional cross-linking, which emphasizes the relevance of trimerbody valence and stoichiometry in the context of agonizing a multimerizing receptor. Importantly, in the presence of EGFR-expressing cells, the trimerbody-4-1BB complexes are further cross-linked, resulting in increased agonistic activity that significantly exceeds that achieved by a 4-1BB IgG cross-linked by FcγRIIb-expressing cells, and was similar to that observed with FcγRIIb-cross-linked urelumab.

When the study was conducted on activated huPBMCs or isolated T cells, the 4-1BB^{N/C}EGFR trimerbody did not increase IFNγ secretion above the basal levels, at any of the concentrations analyzed, in the absence of EGFR-specific cross-linking. These results demonstrate that, in contrast to the results from the Jurkat cell-based hu4-1BB reporter assay, under near physiologic conditions using activated primary T cells the trimerbody-mediated 4-1BB clustering does not provide effective 4-1BB costimulation without additional EGFR-mediated cross-linking. This aspect is particularly relevant, as it shows that effective costimulation is not induced, despite saturating binding of the trimerbody to 4-1BB. This has important implications with regard to off-tumor safety issues, as these results indicate that the trimerbody is not capable of inducing 4-1BB costimulation in TAA-negative tissues.

The humanized EGFR-targeted trimeric 4-1BB-agonistic trimerbody exhibits improved serum stability and a circulatory half-life of nearly 3 days. We hypothesize that strategies aiming to reinvigorate preexisting tumor-specific exhausted T cells (42) could benefit from an intermittent boosting strategy, to reduce systemic exposure and potential toxicity. This may be especially important when using a relatively ubiquitous TAA, such as EGFR, for targeted 4-1BB costimulation. The relatively short half-life combined with the TAA-targeted approach would allow the selective accumulation of the 4-1BB^{N/C}EGFR trimerbody in the tumor area and in tumor cell-infiltrated lymph nodes. In fact, it has been shown that EGFR expression is related with lymph node involvement and tumor grade in colorectal cancer. Also, lymph node-involved colorectal cancers showed higher scores of EGFR staining than control groups (43).

We have recently shown that treatment of immunocompetent transgenic mice expressing huEGFR in the liver (ΔEGFR-tg) (44) with IgG-based anti-mouse 4-1BB agonist resulted in nonspecific immune stimulation and hepatotoxicity (22). In contrast, none of these features were observed in ΔEGFR-tg mice treated with the Fc-free EGFR-specific anti-mouse 4-1BB-agonistic 1D8^{N/C}EGa1 trimerbody (22), despite the fact that the anti-EGFR EGa1 V_{HH} recognize huEGFR and moEGFR. These results further validate the safety profile of Fc-free trimerbodies in systemic cancer immunotherapy protocols. Here, we demonstrated that treatment of huPBMC-driven immunoavatar mice (36) with the anti-4-1BB-agonistic IgG resulted in enhanced activation of adoptively transferred human T cells and exacerbation of hepatic xGVHD. In contrast, treatment with the 4-1BB^{N/C}EGFR trimerbody induced human IFNγ serum levels and liver infiltration similar to that observed in PBS-treated animals.

Despite the limitations of current mouse models for the study of human tumors, such as the development of xGVHD, and insufficient engraftment of some human immune subsets (45), we demonstrated that in huPBMC humanized immunoavatar mouse models of human colorectal cancer and TNBC, 4-1BB^{N/C}EGFR monotherapy provided significant antitumor activity. This effect was confirmed in a humanized PDX model of human NSCLC where treatment with 4-1BB^{N/C}EGFR showed a significant reduction in tumor growth, which was associated with a significant increase in the percentage of CD8⁺ TIL and a substantial improvement of the CD8⁺ T cell/Treg (regulatory T cell) ratio, from 7.5 in the control-treated mice to 50 in the 4-1BB^{N/C}EGFR-treated mice. EGFR can be an effective target for the development of a broadly applicable tumor-specific 4-1BB-mediated immunotherapy. In most solid tumors (including lung, colorectal, prostate, pancreatic, head and neck, liver, renal, urothelial, and endometrial cancers, along with glioblastoma) more than 50% of patients display a moderate to strong expression of EGFR (46). Furthermore, in humanized mice bearing aggressive EGFR⁺ TNBC CLDX expressing high levels of PD-L1, the combination of 4-1BB^{N/C}EGFR with atezolizumab further improved antitumor activity, resulting in 1 of 6 mice undergoing complete regression.

The primary antitumor mechanism of anti-4-1BB IgG₁ mAbs is the activation of CD8⁺ T cells after coengagement of the inhibitory FcγRIIb receptor (47). However, FcγRIIb interactions in the liver are responsible for the liver toxicity of anti-4-1BB IgG_{2a} mAbs (48–50), which primarily act by depleting Tregs through interactions with activating FcγR receptors (47). However, these activating FcγR interactions and the subsequent FcγR-mediated depletion of 4-1BB⁺ cells may compromise antitumor immunity (41). These findings outline a very intricate scenario in which

the number of CD8⁺ TILs, Tregs, and FcγR⁺ cells, along with the relative abundances of activating and inhibitory FcγRs, are likely to determine patient outcomes and must be considered before deciding whether full-length IgG anti-4-1BB agonists are indicated (51). An additional consideration is the competition between administered therapeutic mAbs and endogenous Igs for FcγRs, which will affect the Fc receptor binding of anti-4-1BB agonists and thereby affect their mechanism of action (51). Recently, several IgG-based tumor-targeted 4-1BB agonists have been engineered with effector-silent Fc regions that retain FcRn-driven half-life extension while reducing binding to FcγRs (52, 53), indicating that it can be desirable for a therapeutic antibody to avoid these interactions. However, these mutations may affect mAb stability, and introduce potentially immunogenic sites (54). The trimerbody described in this study has no Fc region and thereby ensures completely FcγR-independent 4-1BB clustering and cross-linking, avoiding residual binding activities shown in “silenced” Fc regions (55), and may be more easily systematized and applied in a clinical setting.

Here, we show that the combination of a humanized tumor-specific Fc-free 4-1BB-agonistic trimerbody with an ICB mAb resulted in a greater therapeutic index compared with either monotherapy. These results demonstrate the benefits of combination therapies using both costimulatory and ICB immunotherapy strategies, and the suitability of the trimerbody platform for enacting costimulatory strategies with high efficacy while avoiding adverse reactions mediated by the Fc region.

Authors' Disclosures

M. Compte reports current employment at Leadartis. A. Erce-Llamazares reports current employment at Leadartis. E.M. Garrido-Martin reports other from PharmaMar and personal fees from Bristol Myers Squibb and Pfizer outside the submitted work. C. Domínguez-Alonso reports grants from the Spanish Minister of Science and Innovation during the conduct of the study. M. Zonca reports grants from Spanish Ministry of Science, Innovation and Universities during the conduct of the study, and reports formal employment at Leadartis. I. Melero reports grants and personal fees from BMS, Roche, AstraZeneca, Biontech, Alligator, Pharmamar, and Genmab, and personal fees from F-Star, Numab, Gossamer, EMD, Amunix, and MSD outside the submitted work. L. Paz-Ares reports personal fees from BMS, AstraZeneca, MSD, Lilly, Roche, Blueprint, Bayer, Mirati, Angem, Jansen, Sanofi, and Pharmamar outside the submitted work. L. Sanz reports grants from Carlos III Health Institute during the conduct of the study and is a co-founder of Leadartis. L. Alvarez-Vallina reports grants from the Spanish Ministry of Science, Innovation and Universities, the CRIS Cancer Foundation, and the Spanish Association Against Cancer during the conduct of the study; in addition, L. Alvarez-Vallina has a patent for WO/2019/234187 licensed to Leadartis SL, and is a co-founder of Leadartis SL. No disclosures were reported by the other authors.

References

- Mahoney KM, Rennett PD, Freeman GJ. Combination cancer immunotherapy and new immunomodulatory targets. *Nat Rev Drug Discov* 2015;14:561–84.
- Chamoto K, Hatae R, Honjo T. Current issues and perspectives in PD-1 blockade cancer immunotherapy. *Int J Clin Oncol* 2020;25:790–800.
- Wei SC, Duffy CR, Allison JP. Fundamental mechanisms of immune checkpoint blockade therapy. *Cancer Discov* 2018;8:1069–86.
- Melero I, Hervas-Stubbs S, Glennie M, Pardoll DM, Chen L. Immunostimulatory monoclonal antibodies for cancer therapy. *Nat Rev Cancer* 2007;7:95–106.
- Kwon BS, Weissman SM. cDNA sequences of two inducible T-cell genes. *Proc Natl Acad Sci U S A* 1989;86:1963–7.
- Saoulli K, Lee SY, Cannons JL, Yeh WC, Santana A, Goldstein MD, et al. CD28-independent, TRAF2-dependent costimulation of resting T cells by 4-1BB ligand. *J Exp Med* 1998;187:1849–62.
- Shuford WW, Klussman K, Tritchler DD, Loo DT, Chalupny J, Siadak AW, et al. 4-1BB costimulatory signals preferentially induce CD8⁺ T cell proliferation and

Authors' Contributions

M. Compte: Conceptualization, resources, formal analysis, supervision, funding acquisition, validation, investigation, methodology, writing—original draft, project administration, writing—review and editing. **S.L. Harwood:** Formal analysis, investigation, methodology, writing—review and editing. **A. Erce-Llamazares:** Validation, investigation. **A. Tapia-Galisteo:** Investigation, methodology. **E. Romero:** Investigation, methodology. **I. Ferrer:** Investigation, visualization, methodology. **E.M. Garrido-Martin:** Investigation, visualization, methodology. **A.B. Enguita:** Investigation, visualization, methodology. **M.C. Ochoa:** Investigation, visualization, methodology. **B. Blanco:** Validation, investigation, visualization, methodology. **M. Oteo:** Investigation, visualization, methodology. **N. Merino:** Investigation. **D. Nehme-Álvarez:** Investigation, visualization. **O. Hangju:** Investigation. **C. Domínguez-Alonso:** Investigation. **M. Zonca:** Investigation, methodology. **A. Ramírez-Fernández:** Investigation. **F.J. Blanco:** Supervision, funding acquisition, investigation, methodology, writing—original draft. **M.A. Morcillo:** Conceptualization, supervision, funding acquisition, investigation, methodology, writing—original draft. **I.G. Muñoz:** Resources, supervision, funding acquisition, validation, investigation, methodology, writing—original draft. **I. Melero:** Conceptualization, resources, supervision, validation, investigation, writing—original draft. **J.L. Rodríguez-Peralta:** Resources, supervision, funding acquisition, validation, investigation, visualization, methodology, writing—review and editing. **L. Paz-Ares:** Resources, supervision, funding acquisition, validation, investigation, visualization, writing—review and editing. **L. Sanz:** Conceptualization, supervision, funding acquisition, investigation, methodology, writing—review and editing. **L. Alvarez-Vallina:** Conceptualization, resources, supervision, funding acquisition, validation, investigation, methodology, writing—original draft, writing—review and editing.

Acknowledgements

We thank M. Glennie and A. Villalobos for reagents, and Diamond Light Source (United Kingdom) for provision of synchrotron radiation at beamline B21. This work was supported by grants from the European Union [IACT Project (602262), H2020-iNEXT (1676)]; the Spanish Ministry of Science, Innovation and Universities and the Spanish Ministry of Economy and Competitiveness (SAF2017-89437-P, CTQ2017-83810-R, RTC-2016-5118-1, RTC-2017-5944-1), partially supported by the European Regional Development Fund; the Carlos III Health Institute (PI16/00357), co-founded by the Plan Nacional de Investigación and the European Union; the CRIS Cancer Foundation (FCRIS-IFI-2018); and the Spanish Association Against Cancer (AECC, 19084). C. Domínguez-Alonso was supported by a predoctoral fellowship from the Spanish Ministry of Science, Innovation and Universities (PRE2018-083445). M. Zonca was supported by the Torres Quevedo Program from the Spanish Ministry of Economy and Competitiveness, co-founded by the European Social Fund (PTQ-16-08340).

The costs of publication of this article were defrayed in part by the payment of page charges. This article must therefore be hereby marked *advertisement* in accordance with 18 U.S.C. Section 1734 solely to indicate this fact.

Received November 28, 2020; revised February 5, 2021; accepted March 26, 2021; published first March 30, 2021.

- lead to the amplification *in vivo* of cytotoxic T cell responses. *J Exp Med* 1997; 186:47–55.
- Wilcox RA, Tamada K, Flies DB, Zhu G, Chapoval AI, Blazar BR, et al. Ligand of CD137 receptor prevents and reverses established anergy of CD8⁺ cytolytic T lymphocytes *in vivo*. *Blood* 2004;103:177–84.
 - Kroon HM, Li Q, Teitz-Tennenbaum S, Whitfield JR, Noone AM, Chang AE. 4-1BB costimulation of effector T cells for adoptive immunotherapy of cancer: involvement of Bcl gene family members. *J Immunother* 2007;30: 406–16.
 - Sabbagh L, Pülle G, Liu Y, Tsitsikov EN, Watts TH. ERK-dependent Bim modulation downstream of the 4-1BB-TRAF1 signaling axis is a critical mediator of CD8 T cell survival *in vivo*. *J Immunol* 2008;180:8093–101.
 - Melero I, Hirschhorn-Cymerman D, Morales-Kastresana A, Sanmamed MF, Wolchok JD. Agonist antibodies to TNFR molecules that costimulate T and NK cells. *Clin Cancer Res* 2013;19:1044–53.

12. Melero I, Shuford WW, Newby SA, Aruffo A, Ledbetter JA, Hellstrom KE, et al. Monoclonal antibodies against the 4-1BB T-cell activation molecule eradicate established tumors. *Nat Med* 1997;3:682-5.
13. Taraban VY, Rowley TF, O'Brien L, Chan HT, Haswell LE, Green MH, et al. Expression and costimulatory effects of the TNF receptor superfamily members CD134 (OX40) and CD137 (4-1BB), and their role in the generation of anti-tumor immune responses. *Eur J Immunol* 2002;32:3617-27.
14. Wilcox RA, Flies DB, Zhu G, Johnson AJ, Tamada K, Chapoval AI, et al. Provision of antigen and CD137 signaling breaks immunological ignorance, promoting regression of poorly immunogenic tumors. *J Clin Invest* 2002;109:651-9.
15. Compte M, Harwood SL, Munoz IG, Navarro R, Zonca M, Perez-Chacon G, et al. A tumor-targeted trimeric 4-1BB-agonistic antibody induces potent anti-tumor immunity without systemic toxicity. *Nat Commun* 2018;9:4809.
16. Li F, Ravetch JG. Antitumor activities of agonistic anti-TNFR antibodies require differential FcγmammaR1B coengagement *in vivo*. *Proc Natl Acad Sci U S A* 2013; 110:19501-6.
17. Xu Y, Szalai AJ, Zhou T, Zinn KR, Chaudhuri TR, Li X, et al. Fc gamma Rs modulate cytotoxicity of anti-Fas antibodies: implications for agonistic antibody-based therapeutics. *J Immunol* 2003;171:562-8.
18. Ascierio PA, Simeone E, Sznol M, Fu YX, Melero I. Clinical experiences with anti-CD137 and anti-PD1 therapeutic antibodies. *Semin Oncol* 2010;37:508-16.
19. Segal NH, Logan TF, Hodi FS, McDermott D, Melero I, Hamid O, et al. Results from an integrated safety analysis of urelumab, an agonist anti-CD137 monoclonal antibody. *Clin Cancer Res* 2017;23:1929-36.
20. Chester C, Sanmamed MF, Wang J, Melero I. Immunotherapy targeting 4-1BB: mechanistic rationale, clinical results, and future strategies. *Blood* 2018;131: 49-57.
21. Mikkelsen K, Harwood SL, Compte M, Merino N, Molgaard K, Lykkemark S, et al. Carcinoembryonic antigen (CEA)-specific 4-1BB-costimulation induced by CEA-targeted 4-1BB-agonistic trimerbodies. *Front Immunol* 2019;10:1791.
22. Compte M, Harwood SL, Martinez-Torrecuadrada J, Perez-Chacon G, Gonzalez-Garcia P, Tapia-Galisteo A, et al. Case report: an EGFR-targeted 4-1BB-agonistic trimerbody does not induce hepatotoxicity in transgenic mice with liver expression of human EGFR. *Front Immunol* 2020;11:614363.
23. Estrada C, Gomez C, Martin C, Moncada S, Gonzalez C. Nitric oxide mediates tumor necrosis factor-α cytotoxicity in endothelial cells. *Biochem Biophys Res Commun* 1992;186:475-82.
24. Cuesta AM, Sanchez-Martin D, Sanz L, Bonet J, Compte M, Kremer L, et al. *In vivo* tumor targeting and imaging with engineered trivalent antibody fragments containing collagen-derived sequences. *PLoS One* 2009;4:e5381.
25. Schmitz KR, Bagchi A, Roovers RC, Van Bergen En Henegouwen PM, Ferguson KM. Structural evaluation of EGFR inhibition mechanisms for nanobodies/VHH domains. *Structure* 2013;21:1214-24.
26. Quintanal-Villalonga A, Molina-Pinelo S, Cirauqui C, Ojeda-Marquez L, Marrugal A, Suarez R, et al. FGFR1 cooperates with EGFR in lung cancer oncogenesis, and their combined inhibition shows improved efficacy. *J Thorac Oncol* 2019;14:641-55.
27. Al-Shamkhani A, Chan HTC, Cragg MS, French RR, Glennie M, Wolchok JD, et al. Immunomodulatory antibodies. Available from: <https://patentscope.wipo.int/search/en/detail.jsf?docId=WO2017077085&tab=PCTBIBLIO>. 2017.
28. Chin SM, Kimberlin CR, Roe-Zurz Z, Zhang P, Xu A, Liao-Chan S, et al. Structure of the 4-1BB/4-1BBL complex and distinct binding and functional properties of utomilumab and urelumab. *Nat Commun* 2018;9:4679.
29. Harwood SL, Álvarez-Cienfuegos A, Nunez-Prado N, Compte M, Hernandez-Perez S, Merino N, et al. ATTACK, a novel bispecific T cell-recruiting antibody with trivalent EGFR binding and monovalent CD3 binding for cancer immunotherapy. *Oncoimmunology* 2017;7:e1377874.
30. Alvarez-Cienfuegos A, Nunez-Prado N, Compte M, Cuesta AM, Blanco-Toribio A, Harwood SL, et al. Intramolecular trimerization, a novel strategy for making multispecific antibodies with controlled orientation of the antigen binding domains. *Sci Rep* 2016;6:28643.
31. Li S, Schmitz KR, Jeffrey PD, Wiltzius JJ, Kussie P, Ferguson KM. Structural basis for inhibition of the epidermal growth factor receptor by cetuximab. *Cancer Cell* 2005;7:301-11.
32. Toutain PL, Bousquet-Melou A. Bioavailability and its assessment. *J Vet Pharmacol Ther* 2004;27:455-66.
33. Nervi B, Rettig MP, Ritchey JK, Wang HL, Bauer G, Walker J, et al. Factors affecting human T cell engraftment, trafficking, and associated xenogeneic graft-vs-host disease in NOD/SCID beta2mnull mice. *Exp Hematol* 2007;35:1823-38.
34. Carroll RG, Carpenito C, Shan X, net-Desnoyers G, Liu R, Jiang S, et al. Distinct effects of IL-18 on the engraftment and function of human effector CD8 T cells and regulatory T cells. *PLoS One* 2008;3:e3289.
35. Mutis T, van Rijn RS, Simonetti ER, arts-Riemsens T, Emmelot ME, van BL, et al. Human regulatory T cells control xenogeneic graft-versus-host disease induced by autologous T cells in RAG2-/-gammac-/- immunodeficient mice. *Clin Cancer Res* 2006;12:5520-5.
36. Sanmamed MF, Rodriguez I, Schalper KA, Onate C, Azpilikueta A, Rodriguez-Ruiz ME, et al. Nivolumab and urelumab enhance antitumor activity of human T lymphocytes engrafted in Rag2-/-IL2Rgamma null immunodeficient mice. *Cancer Res* 2015;75:3466-78.
37. Chen L, Flies DB. Molecular mechanisms of T cell co-stimulation and co-inhibition. *Nat Rev Immunol* 2013;13:227-42.
38. Melero I, Berman DM, Aznar MA, Korman AJ, Perez Gracia JL, Haanen J. Evolving synergistic combinations of targeted immunotherapies to combat cancer. *Nat Rev Cancer* 2015;15:457-72.
39. Baumeister SH, Freeman GJ, Dranoff G, Sharpe AH. Coinhibitory pathways in immunotherapy for cancer. *Annu Rev Immunol* 2016;34:539-73.
40. Wajant H. Principles of antibody-mediated TNF receptor activation. *Cell Death Differ* 2015;22:1727-41.
41. Qi X, Li F, Wu Y, Cheng C, Han P, Wang J, et al. Optimization of 4-1BB antibody for cancer immunotherapy by balancing agonistic strength with FcγmammaR affinity. *Nat Commun* 2019;10:2141.
42. Menk AV, Scharping NE, Rivadeneira DB, Calderon MJ, Watson MJ, Dunstane D, et al. 4-1BB costimulation induces T cell mitochondrial function and biogenesis enabling cancer immunotherapeutic responses. *J Exp Med* 2018;215:1091-100.
43. Mokhtari M, Ardestani MM, Movahedipour M. An immunohistochemical study of EGFR expression in colorectal cancer and its correlation with lymph nodes status and tumor grade. *J Res Med Sci* 2012;17:741-4.
44. Lopez-Luque J, Caballero-Diaz D, Martinez-Palacian A, Roncero C, Moreno-Caceres J, Garcia-Bravo M, et al. Dissecting the role of epidermal growth factor receptor catalytic activity during liver regeneration and hepatocarcinogenesis. *Hepatology* 2016;63:604-19.
45. Morillon YM, Sabzevari A, Schlom J, Greiner JW. The development of next-generation PBMC humanized mice for preclinical investigation of cancer immunotherapeutic agents. *Anticancer Res* 2020;40:5329-41.
46. Uhlén M, Fagerberg L, Hallström BM, Lindskog C, Oksvold P, Mardinoglu A, et al. Tissue-based map of the human proteome. *Science* 2015;347:1260419.
47. Buchan SL, Dou L, Remer M, Booth SG, Dunn SN, Lai C, et al. Antibodies to costimulatory receptor 4-1BB enhance anti-tumor immunity via T regulatory cell depletion and promotion of CD8 T cell effector function. *Immunity* 2018;49: 958-70.
48. Dubrot J, Milheiro F, Alfaro C, Palazon A, Martinez-Forero I, Perez-Gracia JL, et al. Treatment with anti-CD137 mAbs causes intense accumulations of liver T cells without selective antitumor immunotherapeutic effects in this organ. *Cancer Immunol Immunother* 2010;59:1223-33.
49. Niu L, Strahotin S, Hewes B, Zhang B, Zhang Y, Archer D, et al. Cytokine-mediated disruption of lymphocyte trafficking, hemopoiesis, and induction of lymphopenia, anemia, and thrombocytopenia in anti-CD137-treated mice. *J Immunol* 2007;178:4194-213.
50. Vonderheide RH, Glennie MJ. Agonistic CD40 antibodies and cancer therapy. *Clin Cancer Res* 2013;19:1035-43.
51. Álvarez-Vallina L. 4-1BB-mediated cancer immunotherapy: 'mission impossible' for non-engineered IgGs? *Precis Cancer Med* 2019;2:1.
52. Claus C, Ferrara C, Xu W, Sam J, Lang S, Uhlenbrock F, et al. Tumor-targeted 4-1BB agonists for combination with T cell bispecific antibodies as off-the-shelf therapy. *Sci Transl Med* 2019;11:eav5989.
53. Hinner MJ, Aiba RSB, Jaquin TJ, Berger S, Durr MC, Schlosser C, et al. Tumor-localized costimulatory T-cell engagement by the 4-1BB/HER2 bispecific antibody-anticalin fusion PRS-343. *Clin Cancer Res* 2019;25:5878-89.
54. Schlothauer T, Herter S, Koller CF, Grau-Richards S, Steinhart V, Spick C, et al. Novel human IgG1 and IgG4 Fc-engineered antibodies with completely abolished immune effector functions. *Protein Eng Des Sel* 2016;29: 457-66.
55. Vafa O, Gilliland GL, Brezski RJ, Strake B, Wilkinson T, Lacy ER, et al. An engineered Fc variant of an IgG eliminates all immune effector functions via structural perturbations. *Methods* 2014;65:114-26.